Microphotonic forces from superfluid flow - Supplementary Information

1 Photoconvective force

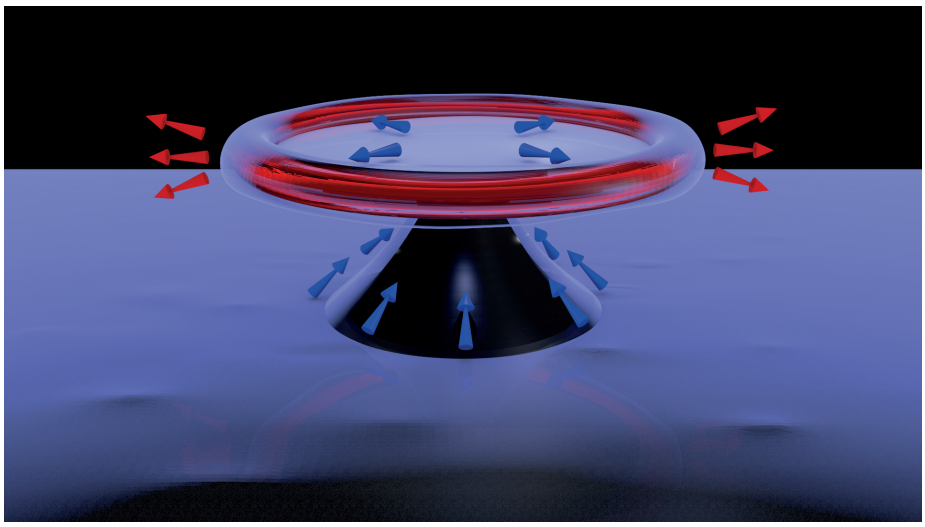

Figure 1: Laser light is evanescently coupled into a microtoroid whispering gallery mode (WGM) and confined to the microtoroid's outer boundary where optical absorption and heat generation takes place (red glow). This increase in temperature causes superfluid helium to flow up the pedestal towards the heat source (thermomechanical effect, blue arrows). At the level of the heat source, superfluid helium is converted into the gas phase (red arrows).

Figure 1 schematically illustrates the experimental conditions. A silica microtoroid rests upon a silicon pedestal on a silicon chip. A thin film of superfluid ^{4}He (<5 nm) covers all surfaces inside the sample chamber, including the microtoroid and the chip. Here we estimate the force on the microtoroid resulting from the light induced flow and evaporation of superfluid helium. To this end, we first carefully estimate the mass flow rate of superfluid helium caused by optical absorption in the microtoroid.

Since the thermal conductivity κ_{sf} of superfluid helium is many orders of magnitude larger than that of silica κ_{SiO_2} at our experimental temperatures [1, 2], we assume in the following that all the heat flow occurs through superfluid convective heat transfer and not through conduction in the silica. Indeed:

$$\frac{\kappa_{sf}\, t_{sf}}{\kappa_{SiO_2}\, t_{SiO_2}} >> 1 \tag{1}$$

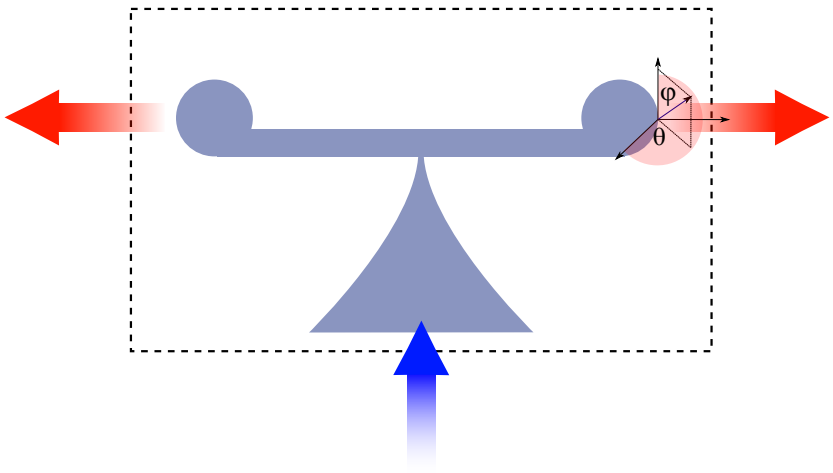

Figure 2: Side view of a microtoroid resonator. Superfluid helium flow originates from the pedestal (blue arrows) and flows towards the hotter microtoroid outer boundary where it is converted into gas phase (red arrows). Note how the velocity of the helium is initially purely vertical before acquiring a radial component.

with t_{sf} and t_{SiO_2} respectively the superfluid film thickness and the silica microtoroid thickness. The validity of this assumption is visible in Fig. 4(a) of the main text, where as soon as the superfluid film boils off the microtoroid is no longer in thermal equilibrium with the cryostat. We consider the steady state case where a heat power P_{abs} is generated through optical absorption at the microtoroid outer boundary. Since in the steady-state neither superfluid nor normal fluid can accumulate on the microtoroid, and any generated normal fluid is viscously clamped to the surface and cannot flow out, this implies that all incoming superfluid must be vaporized. The mass of helium vaporized per second $\dot{m}$ is therefore given by:

$$\dot{m} = \frac{P_{abs}}{L - \langle \mu_{vdw} \rangle + \Delta H} \tag{2}$$

With L $\simeq$ 17.5 kJ/kg the latent heat of vaporization in our experimental conditions [3], $\langle \mu_{vdw} \rangle \simeq -6.4$ kJ/kg the average van der Waals potential of the superfluid film (see section 3.1) and ΔH the change in enthalpy of the superfluid from the cryostat temperature T_0 to the evaporation temperature T_{evap} [1].

In the steady state, all incoming superfluid must arrive through the pedestal. (The effect of condensation of helium on the microtoroid surface is negligible, see section 3.2). Superfluid flow therefore enters the microtoroid with only upwards vertical momentum. At every point on the periphery we consider the evaporation occurs isotropically in the outwards facing half space (see Figure 2), with a root mean square velocity

[1] The change in enthalpy ΔH is small compared to the latent heat of vaporization and can safely be neglected [3].

of:

$$v_{\mathrm{rms}} = \sqrt{\frac{3k_{\mathrm{B}}T_{\mathrm{evap}}}{m_{\mathrm{He}}}} \tag{3}$$

Here $k_{\mathrm{B}} = 1.38\times10^{-23}$ J/K, $m_{\mathrm{He}} = 6.6\times10^{-27}$ kg is the mass of a helium atom and T_{evap} the temperature of the evaporated superfluid atoms ($\simeq$ 1 K). The microtoroid therefore experiences a net inward radial force, due to the change in momentum of the superfluid. The magnitude of this radial force is given by:

$$F_{\mathrm{radial}} = -\frac{\mathrm{d}(mv_{\mathrm{radial}})_{\mathrm{sf}}}{\mathrm{d}t} = \dot{m}v_{\mathrm{rms}}\frac{1}{\pi}\int_{-\pi/2}^{\pi/2}\cos(\theta)\mathrm{d}\theta \times \frac{1}{\pi}\int_{-\pi/2}^{\pi/2}\cos(\phi)\mathrm{d}\phi \tag{4}$$

where the two integral terms account for the projection of the evaporated superfluid's momentum on the radial direction (see Fig. 2). Taking a value for the absorbed power in the microtoroid $P_{\mathrm{abs}} = 1\,\mu$W, Eq. 4 yields $F_{\mathrm{radial}} \simeq -1.3\times10^{-9}$ N.

Eq. 4 predicts both a linear dependence of the force on the laser power, which is what we observe experimentally (see Supplementary Fig. 5), as well as film thickness and pedestal geometry. Note that the vaporization does not produce a net force on the microtoroid in the vertical direction z, as the vaporization is isotropic along z and therefore creates no net change in momentum along z. There is however a force F_z exerted on the microtoroid by the superfluid flow as it changes direction at the junction between the pedestal and the silica disk. The magnitude of this force and its role in our results are discussed in section 3. Finally, by comparing the energy required to evaporate a helium atom to the energy of the incoming photons we can approximate the number of helium atoms N evaporated per absorbed photon

$$N = \frac{\hbar\omega_0}{k_{\mathrm{B}}\left(\mu + \frac{3}{2}T_{\mathrm{evap}}\right)} \tag{5}$$

where ω_0 is the the optical resonance frequency and $\mu = 7.15$ K is the chemical potential [4]. For an evaporation temperature of 1 K this gives a total of 1100 helium atoms evaporated per absorbed photon. Next we compare the magnitude of the radial photo-convective force F_{radial} due to the presence of the superfluid to the more conventional radiation pressure force.

2 Comparison with radiation pressure force

The radial radiation pressure force acting on the microtoroid's outer boundary is given by [5] :

$$F_{\mathrm{RP}} = N_{ph}\hbar\frac{\omega_0}{R} = \frac{PQ}{\omega_0 R} \tag{6}$$

where N_{ph}, P, Q and R are respectively the intracavity photon number, the dropped optical laser power, optical quality factor and the microtoroid major radius. Taking a dropped optical power P equal to the value of P_{abs} previously used (1 μW), we find a radiation pressure force acting radially on the microtoroid outer boundary of $F_{\mathrm{RP}} =$

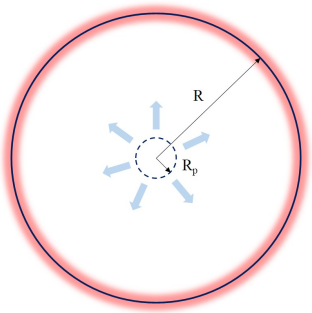

Figure 3: Top view of a microtoroid resonator of radius R, showing the outline of the underlying pedestal in dashed line, and the pedestal radius R_P at the contact point with the silica. Helium flow originates from the pedestal and flows towards the microtoroid outer boundary where the optical absorption and heat generation take place.

1.8×10^{-10} N. (The parameters used in the photoconvective and radiation pressure force calculations are given in Table 3.1).

We find that the magnitude of the superfluid mediated photoconvective force F_{radial} is approximately one order of magnitude larger than the radiation pressure force acting on the microtoroid, in very good agreement with the experimental results, see Fig. 3(a) in the main text.

3 Speed of flow through the pedestal, film boil off and vertical force

From Eq. 2, we can obtain the superfluid volumetric flow rate $\dot{V}$:

$$\dot{V} = \frac{\dot{m}}{\rho} \simeq \frac{1}{\rho}\frac{P_{\text{abs}}}{L - \langle\mu_{\text{vdw}}\rangle} \tag{7}$$

Here ρ is the superfluid helium density. As discussed in section 3.2 all this helium flow must come through the pedestal. The velocity of the fluid is maximal at the narrowest point of the pedestal, at the junction with the reflown silica disk. The speed of the flow through this choke point is therefore:

$$v = \frac{\dot{V}}{2\pi R_{\text{P}}\, t} \tag{8}$$

where t and R_P are respectively the superfluid film thickness and pedestal radius, and $2\pi R_p t$ is the cross sectional area through which superfluid helium can inflow at the level of the pedestal (see Figure 3). In the highly undercut microtoroid used in the experiments, the pedestal radius R_P is estimated (through a Finite Element simulation fitting of the microtoroid mechanical resonance frequencies) to be around 1.65 μm. Taking $P_{\text{abs}} = 1$ μW as in section 1, we get a flow speed in the range of 14 m/s. It is interesting to note that the maximum flow rate at the narrowest part of the pedestal should

ultimately limit the thermal load which can be removed by the superfluid film. In our experiments, film boil off occurs for a power of 2.2 μW (see Fig. 3(b) in the main text), which according to Eq. 8 would correspond to speeds in the 30 m/s range given our uncertainty on the pedestal radius, close to the Landau critical velocity beyond which superfluid helium flow is no longer dissipationless [6]. This could be an explanation for the abrupt film boil off observed in the experiments.

We can also note that the superfluid flow creeping up the pedestal is purely vertical right before reaching the silica disk, at which point it becomes purely horizontal. Therefore, similarly to Eq. 4 we can define a vertical force F_z exerted on the microtoroid at the junction with the pedestal due to the change in momentum of the superflow (not linked to evaporation):

$$F_z = -\frac{\mathrm{d}(mv_z)_{\mathrm{sf}}}{\mathrm{d}t} = \dot{m}v = \frac{\dot{m}^2}{2\rho\,\pi\,R_P\,t} \tag{9}$$

For $P_{\mathrm{abs}} = 1$ μW as previously considered, we find $F_z = 6 \times 10^{-10}$ N. Note that from Eq. 9 and Eq. 2, it appears that this force F_z should have a quadratic dependence upon power P_{abs}, at least for the lowest optical powers, as has been observed in earlier experiments in bulk superfluid [7, 8]. We believe F_z, even though comparable in magnitude to F_{radial}, does not couple efficiently to the mechanical mode of the microtoroid, as the force is applied to a node of the mechanical displacement (see inset of Fig. 2(b) in the main text). It therefore plays a limited role in our experiments, as evidenced also by the linear dependence on power of the superfluid photoconvective force we observe (see Fig. 5). Such a force could however be advantageously leveraged in different designs.

3.1 Van der Waals potential energy

The van der Waals potential μ_{vdw} at a distance d from the substrate is given by (for thin films under 5 nm):

$$\mu_{\mathrm{vdw}} = -\frac{\alpha_{\mathrm{vdw}}}{d^3} \tag{10}$$

where $\alpha_{\mathrm{vdw}} = 2.65{\times}10^{-24}$ m^{5}s^{-2} is the van der Waals coefficient for silica. Considering the first monolayer is clamped to the substrate and does not participate in the heat transport [9], the average chemical potential $\langle\mu_{\mathrm{vdw}}\rangle$ of the flowing superfluid in our experiment is given by:

$$\langle\mu_{\mathrm{vdw}}\rangle \simeq \frac{1}{2-0.35}\int_{x=0.35\mathrm{nm}}^{x=2\mathrm{nm}} \mu_{\mathrm{vdw}}\,(x)\,\mathrm{d}x = -6.4\ \mathrm{kJ/kg} \tag{11}$$

where 0.35 nm is the approximate thickness of the first helium monolayer on the silica microtoroid and 2 nm is the approximate superfluid film thickness. The contribution of the van der Waals potential is non negligible, as it represents close to 36% of the latent heat of vaporization, and is significantly larger than the change in enthalpy of the superfluid. Figure 4 plots μ_{vdw} as a function of the distance to the silica substrate.

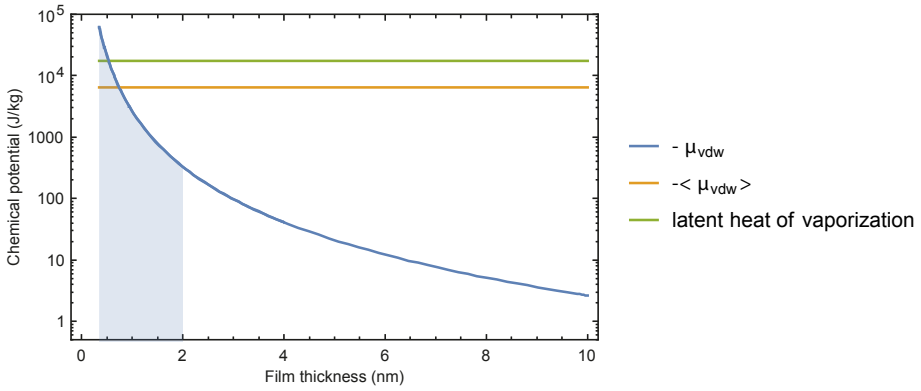

Figure 4: Chemical potential $-\mu_{\mathrm{vdw}}(d)$ as a function of distance d to the silica substrate (blue); shaded region is the thickness of the superfluid film in the experiments over which $\langle\mu_{\mathrm{vdw}}\rangle$ is calculated (orange). In green for comparison, latent heat of vaporization of liquid helium at 500 mK.

Parameter	**Unit**	**Value**
Microtoroid radius	μm	37.5
Pedestal radius (at narrowest)	μm	1.65
Laser wavelength	nm	1555
Photoconvective force		
Absorbed power	μW	1
Latent heat of vaporization L	kJ/kg	17.5
Average van der Waals potential $\langle\mu_{\mathrm{vdw}}\rangle$	kJ/kg	-6.4
Superfluid helium density ρ	kg m^{-3}	145
Mass flow rate $\dot{m}$	kg/s	4×10^{-11}
Flow speed at the pedestal	m/s	$\simeq 14$
Radial photoconvective force F_{radial}	N	1.3×10^{-9}
Vertical photoconvective force F_z	N	6×10^{-10}
Radiation pressure		
Dropped power	μW	1
WGM Optical Q	-	8×10^{6}
Intracavity photons	-	5.2×10^{4}
Radial radiation pressure force	N	1.8×10^{-10}

Table 1: Superfluid parameters and geometric parameters used in the calculations.

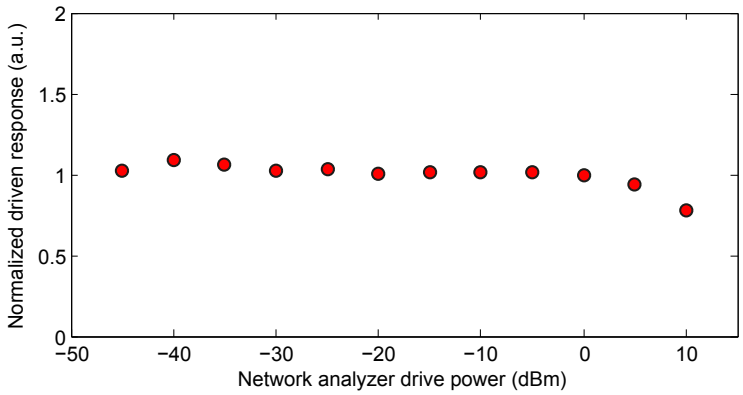

Figure 5: Linear response of the photoconvective force with laser power. We send a 1 μW laser power beam through an electro-optic modulator (EOM) and into the microtoroid and look at the driven response of the microtoroid mode in presence of the superfluid as a function of the drive power on the EOM. (Note that we plot here the *normalized* driven response, which is the driven response divided by the drive power, such that a flat line corresponds to a linear response). The response is essentially linear over a 50 dB range. The drop in response at the highest drive power is due to a saturation of the EOM response.

3.2 Effect of condensation on the microtoroid surface

Here we discuss the influence of the condensation of helium atoms on the microtoroid. The impingement rate r of gas molecules on a surface (in particles per unit area per unit time) is given by the kinetic theory of gases as a function of gas pressure P:

$$r = \frac{\mathrm{P}}{\sqrt{2\pi k_{\mathrm{B}} T m_{\mathrm{He}}}} \tag{12}$$

Even if *every single* helium atom that struck the top and bottom surface of the microtoroid condensed on it, this would correspond to a mass flow rate of:

$$\dot{m}_{\mathrm{condensation}} = r\frac{2\pi R^2}{N_A} M \tag{13}$$

with R the microtoroid major radius, N_A Avogadro's constant and M $\simeq$ 4 g/mol the molar mass of helium. This upper bound is more than one order of magnitude smaller than the mass flow rate due to the thermomechanical effect in our experiments (see Table 3.1). The effect of helium condensation on the surface can therefore safely be neglected. Note as well that condensation events on the surface of the microtoroid are 'energy neutral' as each condensing atom releases its latent heat upon condensation before removing the nearly the same amount as it evaporates at the microtoroid outer boundary, and therefore does not substantially affect the results of Eq. 2.

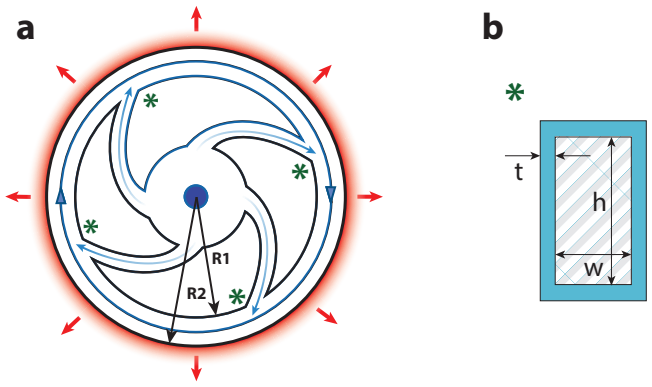

Figure 6: Centrifugal force from superfluid persistent currents. (a) Schematic of the proposed design. (b) cross sectional view of the anchoring points marked by a green asterisk in (a), showing a superfluid layer of thickness t covering a section of thickness h and width w. The superfluid cross section is $2\,(h + w)\,t$.

4 Forces from optically generated superfluid persistent current flow

Here we investigate the prospect of leveraging optically generated persistent current flows in superfluid helium as a means for micromechanical actuation. The concept, in essence a micromechanical analog of Kapitza's famous 'spider' experiment [8], is illustrated in Fig. 6. A ring resonator of outer radius R_2 and inner radius R_1 is connected to an inner pedestal via curved support spokes. As discussed in section 3, optical power dissipated at the level of ring will generate a flow of superfluid up the pedestal and across the spokes towards the hot spot. The superfluid reaching the ring will carry angular momentum and have a speed $v = \dot{V}/A$; where $\dot{V}$ given by Eq. 7 and A is the sum of the cross sections of the superfluid film at the four anchor points marked by a green asterisk in Fig. 6. This flow will generate a persistent current on the ring, marked by the circulating blue arrows. Such persistent currents have already been generated in centimeter scaled superfluid helium thin film resonators through electric driving [10], and have lifetimes of hours up to days [11, 10]. This circulating mass of superfluid is associated to a centrifugal force applied to the ring. In the limit of a narrow annulus $(R2 - R1)/R2 << 1$, this force can simply be expressed as:

$$F_c \simeq m\frac{v^2}{R_2} \tag{14}$$

where m is the mass of superfluid circulating at speed v on the ring. This force could reach large magnitudes: for instance the centrifugal force F_c due to a 10 nm thick superfluid helium film rotating at 30 m/s on a ring with $R_1 = 40$ um and $R_2 = 50$ um is approximately 1.5×10^{-7} N, which corresponds to the radiation pressure force exerted by over 50 million intracavity photons in a resonator of this size.

In the case of a narrow annulus, F_c can be expressed in the steady state as (see Eq.

7):

$$F_c \simeq m\frac{P_{\rm abs}^2}{\rho^2\ (L-\langle\mu_{\rm vdw}\rangle)^2\ A^2\,R} = \frac{4\,\pi\,(R2-R1)\,t}{\rho\ (L-\langle\mu_{\rm vdw}\rangle)^2}\left(\frac{P_{\rm abs}}{A}\right)^2 \tag{15}$$

As evidenced by Eq. 14, the maximum force will be limited by the superfluid critical velocity. However, unlike the radiation pressure force which scales linearly with optical power, F_c scales with the power density $P_{\rm abs}/A$ (see Eq. 15). This means these large persistent current forces can be obtained even with minute optical powers in the nW range, simply by reducing the cross sectional area A, in effect using a constriction to accelerate the flow to large velocities as it enters the ring.

Even more interestingly, thanks to the quantum nature of superflow, the centrifugal force F_c will persist even when the laser power is turned off. Unlike optical radiation pressure and photothermal forces, which typically decay within the range of nanoseconds and microseconds respectively for optical microresonators, the superfluid persistent flow can persist for hours, emulating in a sense the behaviour of a $> 10^{18}$ optical Q cavity. This unique property could have applications in terms of non volatile memories. As an example, let us consider a toroidal resonator of the kind described in [12] (effective mass 5 ng; mechanical frequency $\Omega_M/2\pi = 20$ MHz; $k = 8\times10^4$ N/m spring constant; major radius 35 um). The centrifugal force $F_c \simeq 1\times10^{-7}$ N exerted by a 10 nm thick circulating superfluid helium film on the outer toroidal boundary with speed 30 m/s would be sufficient to produce a shift in the optical resonances frequencies of the resonator of approximately 8 MHz, which is larger than the optical linewidths present in these high Q microtoroidal resonators, potentially enabling such applications as non-volatile optomechanical memories and reconfigurable wavelength routing. (The figures of merit in terms of optical linewidth shifts would be comparable with 200 nm thick ring resonators such as depicted in Fig. 6, whose smaller spring constant would allow for two orders of magnitude larger deflection but that tend have lower optical Qs in the 10^6 range.)

5 Superfluid convective forces in Bulk

Here we briefly address the superfluid convective forces arising from heat transport in bulk superfluid, and point towards optimal parameters required to maximize these forces. Heat transport in bulk liquid helium II can be described in terms of Landau and Tisza's two fluid model [6, 13] where the bulk liquid is divided into a superfluid component of density ρ_s and speed v_s carrying no entropy, and a normal fluid component with density ρ_n and speed v_n which carries the heat. For a steady state linear heat flow, the heat flux $\dot{Q}$ per unit area A is given by [14]:

$$Pd = \frac{\dot{Q}}{A} = \rho S T v_n \tag{16}$$

where $\rho = \rho_n + \rho_s$ is the total bulk density, S the entropy and T the temperature. Additionally, the condition of no mass transport requires [14]:

$$\rho_s v_s + \rho_n v_n = 0 \tag{17}$$

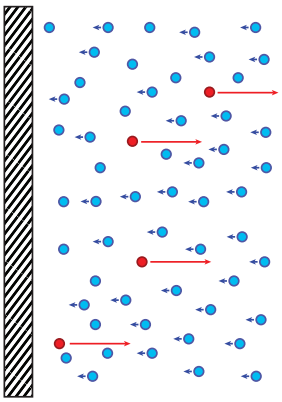

Figure 7: Schematic illustration of heat transport in bulk helium II. Superflow (blue) and normal fluid counterflow (red) at temperatures below 1.9 K such that $\rho_s > \rho_n$. There is no net flow of matter: $\rho_s v_s + \rho_n v_n = 0$; so the superfluid component flow speed v_s (blue arrows) is smaller than the normal fluid flow speed v_n (red arrows).

There is a momentum flux $\rho\vec{v}\cdot\vec{v}$ associated to the flow of each component, such that the total pressure acting upon a heat source is given by [7]:

$$p = \rho_s v_s^2 + \rho_n v_n^2 \tag{18}$$

Since $\rho_s(T)$, $\rho_n(T)$ and $S(T)$ are tabulated functions of temperature [3] (see Figures 8 and 9), for a given T and power density Pd it is possible to completely determine v_s, v_n and p through Eqs. 16, 17 and 18. The flow of each component is associated to a mass flow rate $\dot{m}_s = \rho_s A v_s = \rho_n A v_n$ and an associated kinetic energy, such that one can define an efficiency η relating the kinetic energy acquired by both fluid components per unit time to the heat flux:

$$\eta = \frac{\frac{1}{2}\rho_s v_s^3 + \frac{1}{2}\rho_n v_n^3}{\dot{Q}/A} \tag{19}$$

Here one needs to be careful to enforce the condition $v_s, v_n < v_{\text{crit}}$, with $v_{\text{crit}} \simeq 60$ m/s the Landau critical velocity [14]. Indeed, with $Pd = 10^6$ W/m^2 (for example 1 μW on 1 μm^2) and $T = 0.5$ K, Eq. 16 gives an unphysical normal fluid speed of $v_n = 16.5$ km/s and a heat to kinetic efficiency greater than 1. The function $\eta\left(\dot{Q}/A, T\right)$ with the condition $v_s, v_n < v_{\text{crit}}$ is plotted in Fig. 10. From this figure we see that for low power densities, the heat to kinetic efficiencies are always low, irrespective of the temperature, precluding efficient optical actuation. For higher power densities ($Pd > 10^4$ W/m^2), the theoretical efficiency can reach maximal values in the few tens of percent range, similar to values reported in the literature [15]. There is an optimal temperature at which maximal efficiency is reached, and the value of this optimal temperature depends on the power density. Here we see that enforcing $v_s, v_n < v_{\text{crit}}$ is sufficient to guarantee energy conservation, with $\eta < 1$ over the entire parameter space. Similarly, we can plot the pressure resulting from the heat flow normalized to the power density over the

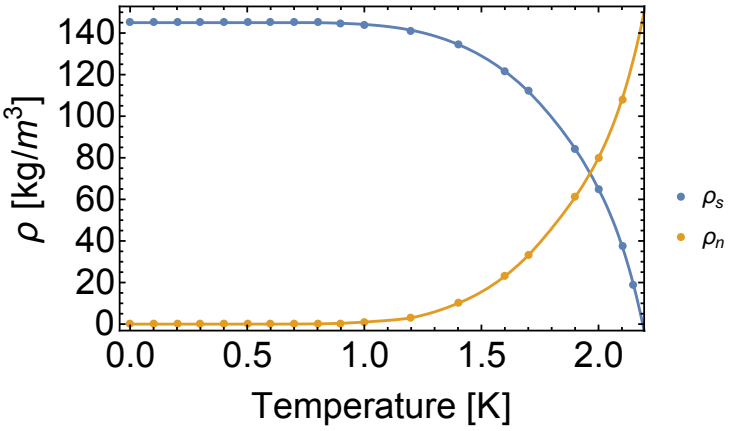

Figure 8: Superfluid and normal fluid component densities ρ_s and ρ_n as a function of bulk temperature. Dots: data from Donnelly et al. [3]; solid line: interpolated function.

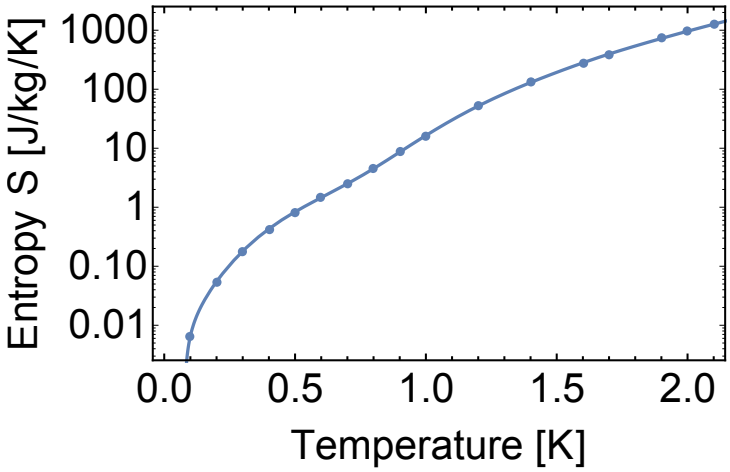

Figure 9: Bulk superfluid entropy S (T) (log scale). Dots: data from [3]; solid line: interpolated function.

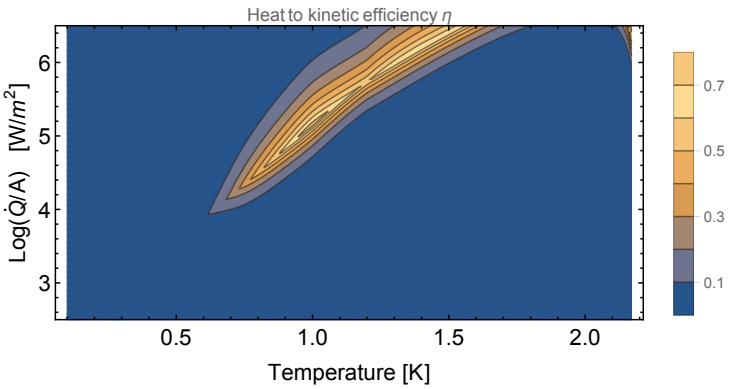

Figure 10: Heat to kinetic energy conversion efficiency η as a function of temperature and power density.

same parameter space:

$$\frac{p}{Pd} = \frac{\rho_s v_s^2 + \rho_n v_n^2}{\dot{Q}/A} \tag{20}$$

This is plotted in Fig. 11, in units of N/W. From this figure we can see that see that simply immersing the current experiment in bulk superfluid helium at for example 1K is not sufficient to allow for large convective forces. Indeed, in the experiment described in the main text, 1 microwatt of heat is dissipated over the toroid's outer surface, corresponding to a power density $Pd = 384$ W/m^2, marked by the red dot in Fig. 11. This power density is too low for strong optical forces, and optical powers of approximately 260 μW would be needed to reach the optimum $Pd \simeq 10^5$ W/m^2 at this temperature. Conversely, this operating regime could also be reached by maintaining $\dot{Q} = 1\,\mu$W but employing a smaller resonator with a surface $A \simeq 10\,\mu$m^2. In the latter case, the theoretical bulk superfluid convective force would be in the range of 2.5×10^{-8} N, approximately 17 times larger than the force demonstrated from the evaporative recoil in superfluid thin films. This increase can be attributed to two factors. First, an increase in the heat to kinetic conversion efficiency η due to the absence of latent heat absorption in the bulk case. Second, this increase can also be understood in terms of N_{He}, the effective number of helium atoms set in motion by each absorbed photon, obtained by dividing the helium atom flow rate by the photon absorption rate:

$$N_{\mathrm{He}} = \frac{\rho_n A v_n}{m_{He}} \times \frac{\hbar\omega_0}{\dot{Q}} = \frac{\rho_n A v_n}{m_{He}} \times \frac{\hbar\omega_0}{A\rho S T v_n} = \frac{\hbar\omega_0}{m_{He}} \times \frac{\rho_n}{\rho S T} \tag{21}$$

From Eq. 21 it appears N_{He} can be simply expressed in terms of the ratio of photon energy to helium atom mass times a function which only depends on temperature; $N_{\mathrm{He}}(T)$ is plotted in Fig. 21. It possesses a maximum of ~8000 near 1 K, approximatevely 7 times larger than the number of atoms set in motion in the evaporative case, resulting in a larger momentum transfer per absorbed photon.

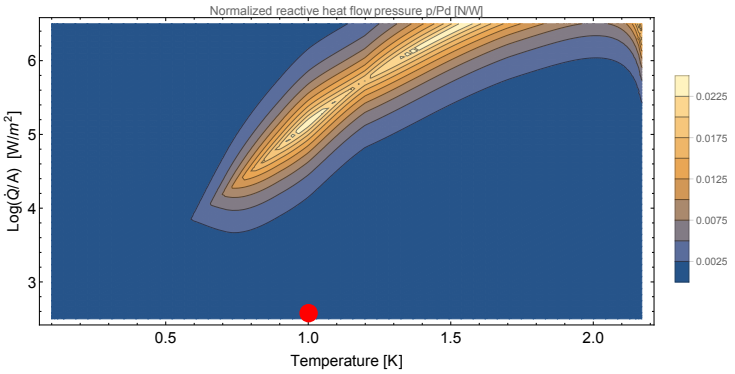

Figure 11: Pressure due to heat flow normalized to power density p/Pd as as a function of temperature and power density. The red dot marks the position of our current experiment if it were immersed in bulk helium at 1 K.

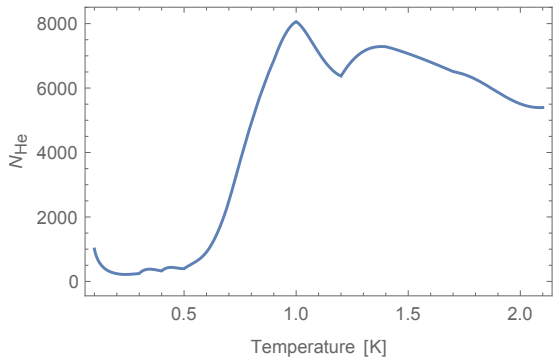

Figure 12: Number of helium atoms set in motion per absorbed photon N_{He}, as a function of bulk temperature (see Eq. 21).

6 Feedback cooling

6.1 Langevin equation approach to the theory of feedback cooling

While the theory of feedback cooling has been extensively covered in numerous publications [16, 17, 18], here a brief theoretical description is presented for clarity. Quite generally the homodyne photocurrent, which is proportional to the phase fluctuations imparted by the mechanical motion, can be expressed as

$$\begin{aligned} \delta i(\omega) &= G_{\mathrm{det}}\delta\tilde{x}(\omega) && (22)\\ &= G_{\mathrm{det}}\left(\delta x(\omega) + \delta N(\omega)\right) && (23)\end{aligned}$$

where $\delta N(\omega)$ is measurement noise and G_{det} is the detection gain given by the detector, interferometer response and optomechanical interaction. In our case the measurement noise is optical shot noise, which is spectrally flat over the region of the mechanics. Deriving a feedback force from this, the photocurrent is fed into an amplitude modulator placed before the microtoroid (see main text Fig. 2(a)). Modulo the cavity response, this results in direct amplitude modulation of the intracavity field and subsequently an applied optically mediated feedback force, namely $F_{\mathrm{fb}}(\omega) \propto \delta i(\omega)$. Combining the effect of detection, actuation and filtering into a single *gain* term the feedback force becomes

$$F_{fb}(\omega) = -g\chi^{-1}(\Omega_m)\delta\tilde{x}(\omega) \tag{24}$$

where g is the feedback gain and the term $\chi^{-1}(\Omega_m)$ has been introduced to make the gain unitless and facilitate factorization into the mechanical susceptibility in later steps. Substituting this expression into the Fourier transformed version of the quantum Langevin equation for the oscillator position yields

$$\delta x(\omega) = \chi'(\omega)\left[F_{th}(\omega) - g\chi^{-1}(\Omega_m)\delta N(\omega)\right] \tag{25}$$

where $\chi'^{-1}(\omega) = m_{\mathrm{eff}}^{-1}\left[\Omega_m^2 - \omega^2 + i\Gamma'_{\mathrm{m}}\Omega_m\right]^{-1}$ is the mechanical susceptibility with modified linewidth $\Gamma'_{\mathrm{m}} = \Gamma_{\mathrm{m}}(1+g)$. The mode temperature can then be estimated from the integrated power spectral density derived from the photocurrent $S_{\tilde{x}\tilde{x}}(\omega) = \langle|\delta\tilde{x}(\omega)|^2\rangle$ giving

$$\begin{aligned} \tilde{T} &= \int_{-\infty}^{\infty} \mathrm{d}\omega\, S_{\tilde{x}\tilde{x}}(\omega) && (26)\\ &= \left(1 - \frac{g(g+2)}{\mathrm{SNR}}\right)\frac{1}{1+g}T_0 && (27)\end{aligned}$$

where T_0 is the initial temperature and the signal-to-noise ratio (SNR) is given by $\mathrm{SNR} = {}^{S_{\tilde{x}\tilde{x}}(\Omega_m)}/_{S_{\mathrm{NN}}(\Omega_{\mathrm{m}})}$. With an initial temperature of $T_0 = 715$ mK this theory accurately describes the behaviour of our system, as can be seen in main text Fig. 5 (solid line). However, since this temperature estimate is derived from the same photocurrent that is applying the feedback, correlations between measurement noise and mechanical motion obscure the actual temperature T. These correlations only occur at high

gain and can be easily accounted for given the SNR and gain. The actual temperature, represented by the dashed line in main text Fig. 5, can be shown to be given by

$$T = \frac{\mathrm{SNR} + \mathrm{g}^2}{\mathrm{SNR} - \mathrm{g}(\mathrm{g}+2)}\tilde{T} \tag{28}$$

resulting in a slightly higher final temperature of 137 mK.

6.2 Magnitude of applied force required to reach the ground state

Feedback cooling can also be treated via a stochastic master equation approach (see for example [19]). This is advantageous since it allows the conditional uncertainty in the state after measurement to be distinguished from uncertainties introduced by the feedback force in the final motional variances. For instance, constraints on the maximum magnitude of the feedback force will limit the final occupancy achieved, even if the measurement conditions the state of the oscillator – prior to feedback – into a perfect coherent state. Here, we use the quantum stochastic master equation approach to determine the magnitude of the feedback force that is required to reach the quantum ground state, following [20]. In [20] it is shown (Eq. (5.40)) that the final occupancy of a high quality oscillator under the action of feedback cooling is given in the rotating wave approximation by

$$\langle\langle \bar{n}_b \rangle\rangle = V_X - \frac{1}{2} + \frac{4\eta C V_X^2}{1+G}, \tag{29}$$

where V_X is the conditional variance of the X quadrature of the oscillator (which in this case is equal to the Y quadrature variance), G is the feedback gain (similar to g above), η is the measurement efficiency, and the double angle brackets signify that the expectation value is taken both over the quantum uncertainty of the state and the classical stochastic diffusion due to imperfections in feedback. In the bad cavity limit C is the optomechanical cooperativity which equals $4g_{om}^2/\kappa\Gamma_m$ with g_{om} being the coherent amplitude boosted optomechanical coupling rate, and κ and Γ_m being the cavity and mechanical decay rates, respectively.

The first two terms in Eq. (29) represent the quantum uncertainty in the conditional state prepared by measurement, while the final term is the uncertainty introduced by imperfections in the feedback. As can be seen, if the feedback gain $G \to \infty$, this last term goes to zero and no degradation is introduced by feedback. More generally, finite feedback gain will lead to some degradation. To determine at what stage constraints in feedback gain preclude reaching the ground state, we take the limit where $C \gg \bar{n}$, with $\bar{n}$ being the thermal occupancy of the bath, and $\eta \to \infty$. In this case, it can be shown from Eq. (5.27) in [20] that to first order in $\bar{n}/C$

$$V_X = \frac{1}{2} + \frac{\bar{n}}{4C}. \tag{30}$$

We see that the conditional quadrature variances approach the zero-point motion level of $1/2$ as $\bar{n}/C \to \infty$. Substituting this expression into Eq. (29) we find that in this limit

$$\langle\langle \bar{n}_b \rangle\rangle = \bar{n}_{meas} + \bar{n}_{feed}, \tag{31}$$

where

$$\bar{n}_{meas} = \frac{\bar{n}}{4C} \tag{32}$$

$$\bar{n}_{feed} = \frac{C+\bar{n}}{1+G}, \tag{33}$$

are, respectively, the phonon occupancies due to imprecision in the measurement and non-ideality of the feedback. For the feedback to be sufficiently good to allow the ground state to be approached, irrespective of the measurement strength, we require

$$\bar{n}_{feed} \ll 1. \tag{34}$$

In the relevant limit where the thermal bath is not already near the ground state (i.e. $\bar{n} \gg 1$), to satisfy this condition clearly requires that $G \gg 1$. Using this and rearranging Eq. (34) for G we find the condition on the gain

$$G \gg C + \bar{n}. \tag{35}$$

As first sight, it may be surprising that this condition depends on the cooperativity. This occurs because, as the cooperativity increases the radiation pressure backaction on the mechanical oscillator also increases. The feedback force must increase to compensate for this additional heating.

The feedback gain G is a dimensionless parameter. Practically speaking, we would, rather, like to know the force in newtons required to approach the ground state. To determine this, we take the derivative of the feedback Hamiltonian in [20] (Eq. (5.32)) with respect to the dimensioned position quadrature $\hat{x} \equiv \hat{X}/\sqrt{2}x_{zp}$, where $x_{zp} = \sqrt{\frac{\hbar}{2m_{\rm eff}\Omega_m}}$ with m_{eff} and Ω_m being the effective mass and resonance frequency of the mechanical oscillator, respctively (note, our X quadrature is labelled X_M in [20]). This provides the x-quadrature force applied by the feedback. A similar result can be obtained for the y-quadrature. For the x-quadrature we find that

$$F_x = \frac{-\hbar\Gamma G\left\langle \hat{X}\right\rangle}{2\sqrt{2}x_{xp}}. \tag{36}$$

It is important to realise that in this expression the mean quadrature position of the mechanical oscillator $\langle\hat{X}\rangle$ is a stochastic variable, the value of which depends on the measurement record and feedback up to the time of measurement. Essentially, this identifies the best-estimate of the position of the oscillator given our knowledge of its past trajectory. In principle, at any given time for a particular trajectory it can take on any value. Therefore, in principle, for any feedback cooling protocol to work perfectly, it must be possible to apply an arbitrarily strong force. In practise, however, $\langle\hat{X}\rangle$ is typically well confined near the origin of phase space, with its standard deviation giving a good indication of the force to achieve effective cooling. In the steady-state, this is given by (see Eq. (5.37) in [20])

$$\Delta\hat{X} \equiv \sqrt{\langle\langle\langle\hat{X}\rangle^2\rangle\rangle} = \sqrt{\frac{4\eta C V_X}{1+G}} \approx \sqrt{\frac{2C}{G}}, \tag{37}$$

where in the approximation we have taken the relevant limit discussed above, where $\eta \to 1$, $C \gg \bar{n}$ and $G \gg 1$. The standard deviation of the applied force is then

$$\Delta F_x = \frac{\hbar\Gamma\sqrt{GC}}{2x_{xp}}. \tag{38}$$

As we found earlier, the requirement to approach the ground state is $G \gg C + \bar{n}$, which since $C \gg \bar{n}$ is also required can be approximated as $G \gg C$. Substituting this into the above expression we obtain the condition on the magnitude of the force

$$\Delta F_x \gg \frac{\hbar\Gamma C}{2x_{xp}}. \tag{39}$$

Let us consider, for the purpose of illustration, the specific case where $C = 16\bar{n}$. In this case, from Eq. (30) the conditional variance of the X-quadrature due to measurement is $V_X = 1/2 + 1/64$ closely approaching the ground state value of $1/2$, while the required feedback force magnitude is

$$\Delta F_x \gg \frac{8\hbar\Gamma\bar{n}}{x_{xp}} \approx \frac{8k_BT}{Qx_{zp}}, \tag{40}$$

where $Q \equiv \Omega_m/\Gamma_m$ is the mechanical quality factor, and we have approximated $\bar{n} = k_BT/\hbar\Omega_m$, valid in the $\bar{n} \gg 1$ limit, with k_B being Boltzmann's constant and T the bath temperature.

Now that we have a relationship for the standard deviation of the force required to bring the mechanical oscillator close to its ground state, we can answer the question as to whether, with our mechanical parameters and the superfluid forces observed within this paper, the ground state can realistically be reached. We note that, of course, substantial enhancements in optomechanical coupling would be required to achieve the separate necessary criterion $C \gg \bar{n}$ to reduce the conditional variance due to measurement to close to the ground state level. Such enhancements have been achieved in other experiments with microtoroids – see for example [21]. Never-the-less, we can still examine whether, once this optomechanical coupling is achieved, the ground state could be approached with the forces achieved in the main paper.

Our microtoroid had a mechanical resonance frequency of $\Omega_m/2\pi = 1.35$ MHz and a dissipation rate of $\Gamma_m/2\pi = 530$ Hz, so that $Q = 2,500$. It's effective mass, calculated by finite-element modelling was $m_{eff} = 25$ ng. Substituting these values into Eq. (40) and taking a bath temperature of 0.7 K, consistent with our experiments, we find that the condition on the standard deviation of the required force $\Delta F_x \gg 60$ pN. This compares favourably to the peak superfluid force magnitude observed in the main text of 1.46 nN. We therefore conclude that superfluid forces are sufficient to approach the ground state with feedback cooling, so long, of course, as the optomechanical coupling is large enough that $C \gg \bar{n}$ (this was not the case for our experiments).

Alternatively, it is illustrative to consider the cross-over point between feedback limited phonon occupancy and measurement conditioning limited phonon occupancy. That is, for what $\bar{n}_{meas}$ does $\bar{n}_{feed} = \bar{n}_{meas}$? Equating Eqs. (32) and (33) and taking the limit that $C \gg \bar{n}$ and $G \gg 1$ we find that this occurs when

$$\bar{n}_{meas} = \frac{1}{2}\sqrt{\frac{\bar{n}}{G}}. \tag{41}$$

Substituting for G using Eq. (38) this becomes

$$\bar{n}_{meas} = \frac{1}{4}\left(\frac{\hbar\Gamma_m\bar{n}}{\Delta F_x x_{xp}}\right)^{2/3} \approx \frac{1}{4}\left(\frac{k_B T}{\Delta F_x Q x_{xp}}\right)^{2/3} \tag{42}$$

Substituting in the parameters above for our experiments, as well as the peak observed superfluid force for ΔF_x, gives an indication of the cross-over occupancy at which feedback imprecision, rather than the residual occupancy from the measurement, would begin to dominate the final phonon occupancy of our device. This occupancy is $\langle\langle \bar{n}_b \rangle\rangle = \bar{n}_{meas} + \bar{n}_{feed} = 2\bar{n}_{meas} = 0.015$, well below the occupancies achieved in any laser cooling experiment to date. This provides further evidence that the forces reported here are sufficient for ground state cooling experiments. We note that this result should be treated as a rough estimate only. An accurate calculation would require a nonlinear model of how the force saturates as it approaches its peak value, rather than simply inserting the peak force into Eq. (42). As far as we are aware, such an approach has not been performed for quantum feedback control of a mechanical oscillator. It would be considerably more difficult than the linear stochastic master equation approach taken in Ref. [20], and is well beyond the scope of this paper.

References

[1] C. E. Chase, "Thermal conduction in liquid helium II. I. Temperature dependence," *Physical Review*, vol. 127, no. 2, p. 361, 1962.

[2] R. C. Zeller and R. O. Pohl, "Thermal conductivity and specific heat of noncrystalline solids," *Physical Review B*, vol. 4, no. 6, p. 2029, 1971.

[3] R. J. Donnelly and C. F. Barenghi, "The observed properties of liquid helium at the saturated vapor pressure," *Journal of Physical and Chemical Reference Data*, vol. 27, no. 6, pp. 1217–1274, 1998.

[4] D. S. Hyman, M. O. Scully, and A. Widom, "Evaporation from superfluid helium," *Physical Review*, vol. 186, pp. 231–238, 1969.

[5] C. Baker, W. Hease, D.-T. Nguyen, A. Andronico, S. Ducci, G. Leo, and I. Favero, "Photoelastic coupling in gallium arsenide optomechanical disk resonators," *Opt. Express*, vol. 22, pp. 14072–14086, June 2014.

[6] L. Landau, "Theory of the superfluidity of helium II," *Physical Review*, vol. 60, no. 4, p. 356, 1941.

[7] H. E. Hall, "The Inertia of Heat Flow in Liquid Helium II," *Proc. Phys. Soc. A*, vol. 67, p. 485, June 1954.

[8] P. L. Kapitza, *Collected papers of PL Kapitza*. Pergamon Press, 1964.

[9] J. H. Scholtz, E. O. McLean, and I. Rudnick, "Third Sound and the Healing Length of He II in Films as Thin as 2.1 Atomic Layers," *Phys. Rev. Lett.*, vol. 32, pp. 147–151, Jan. 1974.

[10] F. M. Ellis and L. Li, "Quantum swirling of superfluid helium films," *Physical review letters*, vol. 71, no. 10, p. 1577, 1993.

[11] I. Rudnick, H. Kojima, W. Veith, and R. S. Kagiwada, "Observation of Superfluid-Helium Persistent Current by Doppler-Shifted Splitting of Fourth-Sound Resonance," *Phys. Rev. Lett.*, vol. 23, pp. 1220–1223, Nov. 1969.

[12] G. Anetsberger, R. Rivire, A. Schliesser, O. Arcizet, and T. J. Kippenberg, "Ultralow-dissipation optomechanical resonators on a chip," *Nature Photonics*, vol. 2, pp. 627–633, Oct. 2008.

[13] L. Tisza, "The theory of liquid helium," *Physical Review*, vol. 72, no. 9, p. 838, 1947.

[14] D. R. Tilley and J. Tilley, *Superfluidity and superconductivity*. CRC Press, 1990.

[15] A. Hofmann, "Method for cooling an object with the aid of superfluid helium (he ii) and apparatus for implementing the method," 1987.

[16] K. H. Lee, T. G. McRae, G. I. Harris, J. Knittel, and W. P. Bowen, "Cooling and control of a cavity optoelectromechanical system," *Physical Review Letters*, vol. 104, no. 12, p. 123604, 2010.

[17] M. Poggio, C. L. Degen, H. J. Mamin, and D. Rugar, "Feedback cooling of a cantilever's fundamental mode below 5 mk," *Physical Review Letters*, vol. 99, no. 1, p. 017201, 2007.

[18] M. Pinard, P. F. Cohadon, T. Briant, and A. Heidmann, "Full mechanical characterization of a cold damped mirror," *Physical Review A*, vol. 63, no. 1, p. 013808, 2000.

[19] A. C. Doherty, A. Szorkovszky, G. Harris, and W. Bowen, "The quantum trajectory approach to quantum feedback control of an oscillator revisited," *Philosophical Transactions of the Royal Society of London A: Mathematical, Physical and Engineering Sciences*, vol. 370, no. 1979, pp. 5338–5353, 2012.

[20] W. P. Bowen and G. J. Milburn, *Quantum Optomechanics*. CRC Press, 2016.

[21] E. Verhagen, S. Deléglise, S. Weis, A. Schliesser, and T. J. Kippenberg, "Quantum-coherent coupling of a mechanical oscillator to an optical cavity mode," *Nature*, vol. 482, no. 7383, pp. 63–67, 2012.